FULL PAPER

QUANTUM CHEMISTRY WILEY

Quantum mechanical modeling of Zn-based spinel oxides: Assessing the structural, vibrational, and electronic properties

Marisa C. Oliveira[1] 🆔 | Renan A. P. Ribeiro[2,3] 🆔 | Elson Longo[2] |
Mauricio R. D. Bomio[1] | Sergio R. de Lázaro[4]

[1]LSQM—Laboratory of Chemical Synthesis of Materials—Department of Materials Engineering, Federal University of Rio Grande do Norte, Natal, Rio Grande do Norte, Brazil

[2]CDMF-LIEC, Federal University of São Carlos, São Carlos, São Paulo, Brazil

[3]Departament of Chemistry, State University of Minas Gerais, Divinópolis, Minas Gerais, Brazil

[4]Department of Chemistry, State University of Ponta Grossa, Ponta Grossa, Puerto Rico, Brazil

Correspondence
Marisa C. Oliveira, LSQM—Laboratory of Chemical Synthesis of Materials, Department of Materials Engineering, Federal University of Rio Grande do Norte, P.O. Box 1524, 59078-900, Natal, RN, Brazil.
Email: marisa-coliveira@hotmail.com

Abstract

The structural, electronic, and vibrational properties of two leading representatives of the Zn-based spinel oxides class, normal ZnX_2O_4 (X = Al, Ga, In) and inverse Zn_2MO_4 (M = Si, Ge, Sn) crystals, were investigated. In particular, density functional theory (DFT) was combined with different exchange-correlation functionals: B3LYP, HSE06, PBE0, and PBESol. Our calculations showed good agreement with the available experimental data, showing a mean percentage error close to 3% for structural parameters. For the electronic structure, the obtained HSE06 band-gap values overcome previous theoretical results, exhibiting a mean percentage error smaller than 10.0%. In particular, the vibrational properties identify the significant differences between normal and inverse spinel configurations, offering compelling evidence of a structure-property relationship for the investigated materials. Therefore, the combined results confirm that the range-separated HSE06 hybrid functional performs the best in spinel oxides. Despite some points that cannot be directly compared to experimental results, we expect that future experimental work can confirm our predictions, thus opening a new avenue for understanding the structural, electronic, and vibrational properties in spinel oxides.

KEYWORDS

DFT, electronic structure, hybrid functional, Zn-based spinel oxides

1 | INTRODUCTION

The Zn-based spinel class of oxides, ZnB_2O_4, in which B represents different cations and O is oxygen, has a cubic symmetry with a space group *Fd-3m*. The spinels comprise of a wide variety of compounds, which are commonly divided into two kinds of structures: *normal* and *inverse* structures. For the *normal* structure, the Zn atoms occupy 1/8 of the tetrahedral sites, whereas the B-site cation occupies half of the octahedral sites. On the other hand, for the *inverse* structure, the tetrahedral voids are filled by the Zn cations, whereas the octahedral voids are occupied by both Zn and B cations, alternating between [ZnO4] tetrahedral and [ZnO6]/[BO6] octahedral sites in the crystal lattice.[1–5]

From this point of view, zinc aluminate ($ZnAl_2O_4$),[6,7] zinc gallate ($ZnGa_2O_4$),[5,8] and zinc indate ($ZnIn_2O_4$)[9,10] compounds are *normal* spinels and belong to this fascinating material family. In contrast, zinc silicate (Zn_2SiO_4),[11] zinc germinate (Zn_2GeO_4),[12] and zinc stannate (Zn_2SnO_4)[13,14] generally crystallize into a cubic *inverse* spinel crystal structure.

Spinel oxide compounds form an extensive range of ceramic compounds with excellent interesting mechanical, electrical, optical, magnetic, elastic, and structural properties.[15–18] Many AB_2O_4 spinels exemplified by zinc aluminate ($ZnAl_2O_4$) crystallize in the cubic spinel structure, belonging to the *Fd-3m* space group. $ZnAl_2O_4$ shows an attractive ceramic in electrical, electronic, and magnetic properties and can be used for sensors, luminescent and catalytic applications.[3,19–21] However, the luminescence behavior of $ZnAl_2O_4$ nanoparticles will be more specific due to the change of energy band-gap and defects in the size of particles.[22,23] Fortunately, $ZnAl_2O_4$ is currently an alternative material for hydrogen generation.[7]

$ZnGa_2O_4$ is also an AB_2O_4 spinel-type crystal structure, has received extensive attention from researchers as a good luminescent material matrix, and shows various emission colors when doped with different transition metal ions or rare-earth ions, such as Cr^{3+}.[24–27] Furthermore, the correlation between microwave dielectric properties, changes in the crystal structure, and cation distribution of Cr-doped $ZnGa_2O_4$ have been systematically investigated.[28] Besides, pure and In-doped $ZnGa_2O_4$ has been reported for its promising photo-induced applications.[9,29,30]

On the other hand, inverse spinel, such as the Zn_2SiO_4,tructure, is an extremely versatile and very attractive host matrix for phosphors because of its excellent optical property on the microstructure, morphology, and binding energy. These applications have stimulated many investigations on the spectroscopic properties of transition metal and rare-earth ions-doped Zn_2SiO_4 phosphors.[31–35] In particular, the doped Zn_2SiO_4 phosphors are widely applied in luminescence thermometry, electroluminescent devices, fluorescent lamps, plasma display panels, white light-emitting diodes, cathode ray tubes, and optoelectronic devices.[36]

Germanium-based composites, such as zinc orthogermanate (Zn_2GeO_4), have been reported for potential applications in light-emitting devices, photocatalysis, and lithium-ion batteries, in which Zn_2GeO_4 materials can be doped with rare-earth ions or transition metal ions to show excellent properties. In addition, as an essential wide band-gap photocatalyst, Zn_2GeO_4 has demonstrated superior activities for water splitting, degradation of pollutants, and photoreduction of CO_2.[37–50] Moreover, the ability to modulate in vitro inflammatory mediators and in vivo acute inflammation of Mn-doped Zn_2GeO_4 was evaluated for the first time by V. Y. Suzuki et al.[51]

Zinc stannate (Zn_2SnO_4) is an n-type transparent conducting oxide and was investigated as a transparent conducting oxide in electro-optical devices, owning to its optical transparency and electrical conductivity.[52] Its composition has higher electron mobility (10-30 cm^2 V^{-1} second^{-1}), a wide optical band-gap of approximately 3.6 eV, and a relatively low refractive index of ~2.0 in the visible spectrum. Chemically, it is stable with regard to the acid, base solution, and polar organic solvents.[53,54] Because of its outstanding electrical and optical properties, lead researchers use it as gas sensors,[55] Li-ion batteries [56] dye-sensitized solar cells,[57,58] and photocatalysis.[59–62] In addition, Zn_2SnO_4 has excellent potential for synthesis in different morphologies.[63]

It has recently become possible to compute an essential number of electronic and structural parameters of solids with high accuracy from first-principle calculations.[64] These kinds of developments in computer simulations have opened up many interesting and exciting possibilities in condensed matter studies. Moreover, several studies on the electrical and optical properties of spinel compounds have been reported, which are of particular interest from the viewpoint of experimental and theoretical techniques.[65–67]

The calculations of the electronic band profile of Zn-based spinel compounds have been studied using local density approximation (LDA) and generalized gradient approximation (GGA).[17,68,69] Despite these research efforts, many inquiries remain unclear. These facts have inspired us to perform a more comprehensive investigation concerning the structural and electronic properties of this Zn class of materials in their cubic phase to explore their promising applications.

Furthermore, to optimize the use of spinel structure metal oxide, mainly adjusted by modification of Al, Ga, In, Si, Ge, or Sn metals, it is essential to understand the physical and chemical properties of these materials. Understanding the optical, electronic, and structural properties of spinel oxide is a crucial step not only for the understanding of surface-related phenomena and processes such as gas sensing, thin-film growth, and catalysis but also for the understanding of the oxide-oxide interfaces and metal-oxide properties.

In this paper, the search is highlighted with current progress on first-principles calculations performed for Zn-based spinel compounds for exploring the effect of changing B from ZnX_2O_4 to x = Al, Ga, In and from Zn_2MO_4 to M = Si, Ge, Sn in terms of structural stability in cubic phase and its corresponding electronic and vibrational properties. We use the optimized crystalline structures to investigate the band structures and density of states (DOS) to explore the electronic structure of these compounds, providing a comprehensive overview and an accurate approximation for addressing practical technological applications of wide band-gap compounds.

2 | COMPUTATIONAL DETAILS

Quantum mechanical calculations in the framework of the density functional theory (DFT) were carried out using four B3LYP,[70,71] HSE06,[72] PBE0,[73] and PBESol[74,75] hybrid (DFT/HF, HF = Hartree-Fock) functionals implemented in the CRYSTAL17 code.[76] Here, Zn_2MO_4, in which M is composed of Si, Ge, and Sn atoms, is depicted as an inverse spinel represented in Figure 1A,B. However, ZnX_2O_4, where X is composed of Al, Ga, and In atoms, were simulated in a *normal* spinel configuration considering the primitive unit cell of the *Fd-3m* cubic symmetry, containing

FIGURE 1 Conventional and primitive *Fd-3m* crystallographic unit cell for (A-C) Zn_2MO_4 (M = Si, Ge, Sn) inverse spinel materials and (B-D) ZnX_2O_4 (X = Al, Ga, In) *normal* spinel materials. The green, orange, blue, and red balls represent Zn, X, M, and O atoms, respectively. The green, orange, and blue polyhedral represent the $[ZnO_4]$, $[ZnO_6]$, $[XO_6]$, and $[MO_6]$ clusters, respectively
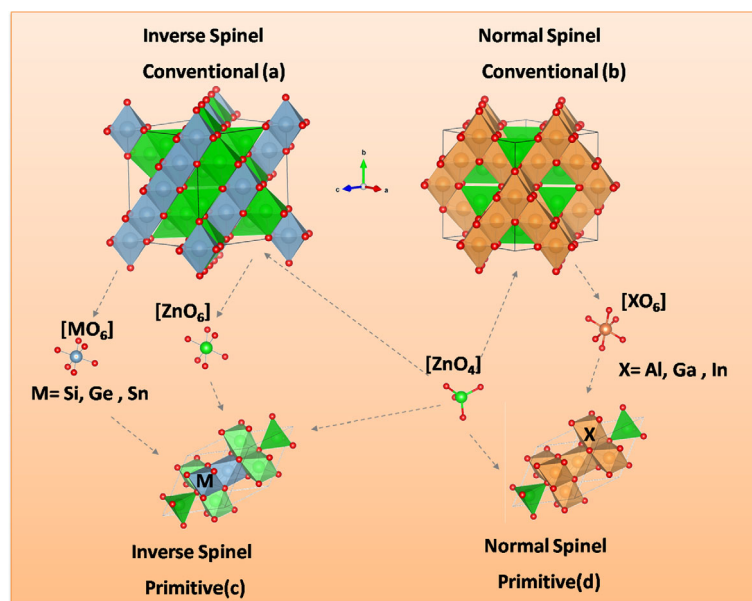
14-atom units, as shown in Figure 1C, and a conventional unit cell, as shown in Figure 1D. In this case, the normal spinel unit cell is composed of tetrahedral $[ZnO_4]$ and octahedral $[XO_6]$ (X = Al, Ga, In) clusters, while the inverse spinel unit cell contains tetrahedral $[ZnO_4]$ and mixed $[ZnO_6]$/$[MO_6]$ (M = Si, Ge, Sn) clusters.

For all materials, Zn_2MO_4 and ZnX_2O_4, atomic positions, and unit cell parameters were relaxed as a function of the Total Energy system. The convergence criteria for mono- and bielectronic integrals were both set to 10^{-8} Hartree. In contrast, the root-mean square (RMS) gradient, RMS displacement, maximum gradient, and maximum displacement were set to 3×10^{-4}, 1.2×10^{-3}, 4.5×10^{-4}, and 1.8×10^{-3} a.u., respectively. Regarding the density matrix diagonalization, the reciprocal space net was described by a dense mesh consisting of a shrinking factor set to $4 \times 4 \times 4$, corresponding to 8 *k*-points for ZnX_2O_4 and 18 *k*-points Zn_2MO_4 under the Monkhorst-Pack method.[77] The accuracy in evaluating the Coulomb and exchange series was controlled by five thresholds, for which the adopted values are 10^{-8}, 10^{-8}, 10^{-8}, 10^{-8}, and 10^{-14}. In all calculations, Zn,[78] Al,[79] Ga,[80] Si,[81] and Ge[82] atoms were described by the standard all-electron 86-411d31G, 85-11G*, 86-4111d41G, 66-21G*, and 9-7631(511d)G basis sets, respectively, as well as for the O atoms described by Gaussian basis sets of Triple-Zeta Valence with Polarization.[83] The In[84] and Sn[85] atoms were described using pseudopotential basis sets. The band structures were calculated for 80 K points along the Γ (0; 0; 0), L (½, ½, ½), and X (½, 0, ½) high-symmetry points of the Brillouin zone. Diagrams of the density of state (DOS) were obtained to analyze the corresponding electronic structure.

3 | RESULTS

3.1 | Structural parameters

At ambient pressure, ZnX_2O_4 are ternary compounds that belong to the *Fd-3m* (227) space group with AB_2O_4 stoichiometry (Figure 1A). The *A* cations are tetrahedrally coordinated, whereas the *B* cations in $[BO_6]$ are octahedral. The Zn atoms are located at tetrahedral sites (8a in Wyckoff notation, point symmetry), whereas X (X = Al, Ga, and In) atoms are situated at octahedral sites (16d in Wyckoff notation point symmetry) and the O atoms at positions (u,u,u) (32e in Wyckoff notation point symmetry) of a face-centered cubic structure.[86] The $[AO_4]$ tetrahedral units are comprised of the A cation at the center and four oxygen atoms in the nonadjacent corners, and no sides are in contact one with another. The $[XO_6]$ octahedral units are structured from an X cation at the center and surrounded by six oxygen atoms, with two each along each dimensional axis.

On the other hand, octahedral units share a single edge with an adjacent octahedral unit. However, for the Zn_2MO_4 inverse spinel structure, the tetrahedral voids are occupied by the M atoms, and the octahedral voids are occupied by both Zn and M atoms (Figure 1B). The spinel crystal structure is characterized only by the lattice parameter (*a*) and the internal parameter (*u*).

To assess the validity of the different exchange-correlation functionals to simulate structural properties, we calculated the mean percentage error for lattice parameters and for unit cell volume to evaluate the agreement with experimental results, as presented in Figure 2A. In particular, it was observed that PBE0 hybrid functional showed the smallest deviations from the experimental results among the investigated functionals, followed by PBESOL, HSE06, and B3LYP.
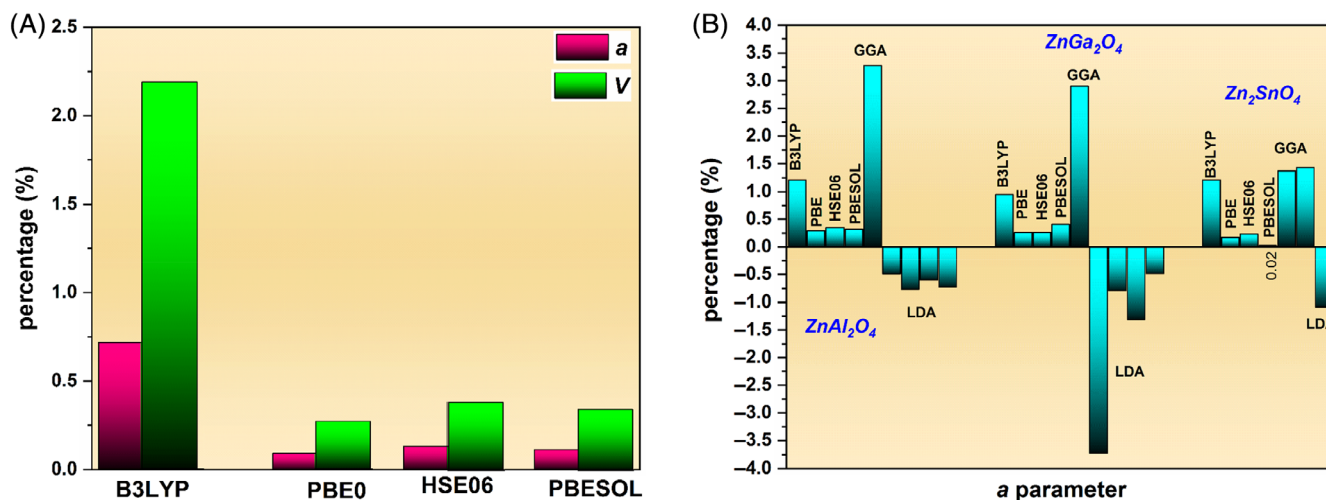
FIGURE 2 A, Calculated mean percentage error for the lattice parameters and unit cell volume using density functional theory (DFT) and the hybrid functional of the ZnX_2O_4 (X = Al, Ga, In) and Zn_2MO_4 (M = Si, Ge, Sn) materials. B, Comparison between calculated percentage error for the lattice parameters using hybrid functional (this work) and previously reported values using local/semilocal formalisms

From an experimental and theoretical point of view, $ZnAl_2O_4$, $ZnGa_2O_4$, and Zn_2SnO_4 have been extensively reported in the literature, helping in the comparison between the hybrid functional results and other theoretical works using the local (LDA) and non-local (GGA) functionals, as shown in Figure 2B. In this case, the experimental lattice parameters were reported as a = 8.086 Å for $ZnAl_2O_4$; a = 8.330 Å for $ZnGa_2O_4$[87]; and a = 8.681 Å for Zn_2SnO_4.[14] It was generally observed that hybrid functionals more accurately reproduced the structural parameters for $ZnAl_2O_4$, $ZnGa_2O_4$, and Zn_2SnO_4 materials in comparison to local/semilocal formalisms, indicating that such a kind of exchange-correlation treatment is indicated more for the reproduction of the spinel materials.

Although these hybrid functionals have shown greater efficacy to simulate the lattice parameters (a = b = c), the obtained errors are less than 0.2% for PBE0, PBESOL, and HSE06. Therefore, there is good agreement between our hybrid functional results for these spinels and previous experimental data. Although the PBE0 and PBESOL functionals have shown good and acceptable structural parameters, these functionals exhibit discrepant band-gap energy value when compared to the experimental results. In contrast, the HSE06 functional describes the structural parameters (a = b = c) as the band-gap energy with the best average accuracy to the experimental Zn-based spinel oxides. More details of the electronic properties are shown in Section 3.2.

The lattice parameters, unit cell volume, internal parameter, and bond distance results from the DFT benchmark for spinel materials using the HSE06 hybrid functional are shown in Table 1.

The optimization of the structural parameters was performed using the selected atomic basis with the HSE06 hybrid functional, as described in Table 1. We found that the lattice parameter increases with the X atomic group (Al, Ga, and In) and M (Si, Ge, and Sn). In addition, the u internal parameter values for the oxygen atoms showed good agreement for the experimental model, as well as for other calculation models. However, Zn_2SiO_4 and Zn_2GeO_4 with the Fd-$3m$ space group have not been reported before by theoretical or experimental data.

The Zn for the normal spinel ($[A^{2+}][B^{3+}]_2O_4$, i = 0) was located in the tetrahedral sites, while trivalent cations (Al, Ga, and In) were presented in octahedral sites. On the other hand, four-valent cations (Si, Ge, and Sn) in the inverse spinel ($[A^{2+}][A^{2+}B^{4+}]O_4$, i = 1) occupy the octahedral sites, whereas the divalent cation (Zn) was equally distributed to the tetrahedral and octahedral sites. As depicted in Table 1, the Zn-O bond length in the tetrahedral structure is about 1.95 to 2.04 Å. It is possible to observe increasing ionic radii in the sequence 0.53 Å (Al) < 0.60 Å (Ga) < 0.80 Å (In), while the bond length was increased in the octahedral site by about 1.91 to 2.16 Å, following the order of $ZnIn_2O_4$ > $ZnGa_2O_4$ > $ZnAl_2O_4$. Besides, the zinc cation in inverse spinel can occupy both octahedral and tetrahedron sites, and a change in bond length occurs, while the same tendency is not observed for the normal spinel. However, it was possible to note that the increase of the ionic radii in the inverse spinel materials is 0.40 Å (Si), 0.53 Å (Ge), and 0.69 Å (Sn); then, the bond length was increased in the octahedral site by about 1.75 to 2.05 Å, following the order of Zn_2SnO_4 > Zn_2GeO_4 > Zn_2SiO_4.

3.2 | Electronic properties

In order to investigate the electronic structure of normal and inverse Zn-based spinel oxide structures, theoretical results for band structure and DOS profiles were analyzed. First, we will discuss the effect among the exchange-correlation functionals in the band-gap values in ZnX_2O_4 (X = Al, Ga, In) and Zn_2MO_4 (M = Si, Ge, Sn) materials. For the $ZnAl_2O_4$ normal spinel, conventional exchange-correlation functionals (B3LYP, PBE0, HSE06, and PBESOL) were noted to suggest band-gap values of around 4.29 to 7.00 eV. The results overestimate the experimental band-

TABLE 1 Results for lattice parameter (Å), volume (Å^3), internal parameter u, and bond distances (d_{Zn-O} and d_{B-O}) in (Å) for the HSE06 hybrid functional

Spinel compounds	Lattice parameter (a = b = c)	Volume	u	d_{Zn-O}	d_{B-O}	Reference
$ZnAl_2O_4$	8.107	532.82	0.264	1.958	1.917	This work
Others works	8.091	529.67	0.27	1.97	1.920	[69]
	8.086	528.69	0.260	1.940	1.920	[87]
	8.091	529.67	0.265	1.966	1.906	[88]
	8.020	515.84	0.263	1.929	1.901	[89]
	8.079	527.31	—	—	—	[90]
$ZnGa_2O_4$	8.359	584.06	0.261	1.983	1.994	This work
Others works	8.341	580.30	0.259	1.949	2.004	[89]
	8.289	569.51	0.260	1.950	1.987	[91]
	8.330	578.00	0.261	1.97	1.990	[87]
	8.603	636.72	0.261	2.032	2.057	[68]
$ZnIn_2O_4$	8.900	704.97	0.257	2.039	2.162	This work
Others works	9.092	751.58	0.255	2.055	2.224	[68]
	8.868	967.39	0.380	—	—	[92]
	8.869	697.62	0.254	—	—	[93]
	8.929	712.074	0.255	—	—	[17]
	9.076	747.62	0.255	—	—	[94]
Zn_2SiO_4	8.108	533.01	0.207	2.131 $O_{(=2x)}$a 2.026 $O_{(=4x)}$a 1.942 $T_{(=2x)}$b 2.039 $T_{(=2x)}$b	1.750 $O_{(=2x)}$a 1.879$O_{(=4x)}$a — — —	This work
Others work	8.075	526.53	0.243	—	—	[95]
Zn_2GeO_4	8.342	580.51	0.243	2.142 $O_{(=2x)}$a 2.049 $O_{(=4x)}$a 1.954 $T_{(=2x)}$b 2.039 $T_{(=2x)}$b	1.859 $O_{(=2x)}$a 1.965 $O_{(=4x)}$a — — —	This work
Others work	8.354	583.02	0.386	—	—	[96]
	8.349	582.16	—	—	—	[97]
Zn_2SnO_4	8.701	658.73	0.241	2.164 $O_{(=2x)}$a 2.100 $O_{(=4x)}$a 1.997 $T_{(=2x)}$b 2.038 $T_{(=2x)}$b	2.046 $O_{(=2x)}$a 2.102 $O_{(=4x)}$a — — —	This work
	8.76	672.22	—	2.098 2.041	2.041 —	[98]
	8.62	640.50	0.241	—	—	[99]
Others work	8. 650	647.21	—	—	—	[100,101]
	8.658	649.01	—	—	—	[52]
	8.681	654.19	—	—	—	[14]
	8.587	633.20	—	—	—	[102]
	8.805	682.72	—	—	—	[102]
	8.657	648.88	—	—	—	[13,92]

Note: a and b refer to octahedral (O) and tetrahedral (T) coordinates, respectively; the value in parenthesis refers to the multiplicity of bond length.
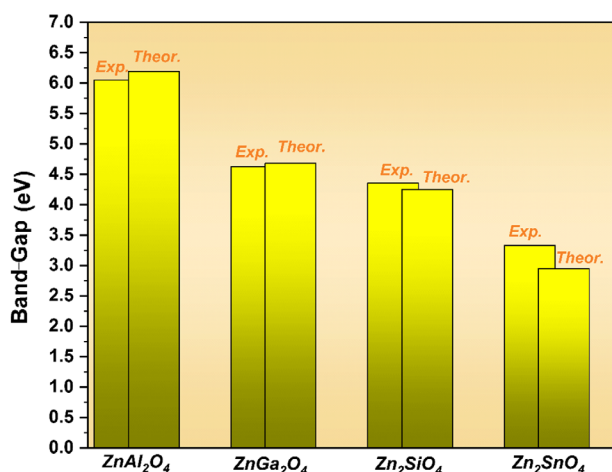
FIGURE 3 Mean error percentage for band-gap energy using the HSE06 functional regarding experimental results

gap energy from 2.31 up to 15.76% for HSE06, B3LYP, and PBE0 functionals, respectively, except for PBESOL, which is 29% lower than the experimental band-gap energy. The band-gap energy for the $ZnGa_2O_4$ was calculated to be around 2.83 to 5.37 eV, and it was noted that HSE06, B3LYP, and PBE0 functionals overestimate the experimental band-gap energy by 1.36 to 16.27%. In contrast, PBESOL underestimates the experimental band-gap energy by 38.65%. However, no experimental data have been reported for $ZnIn_2O_4$, thus making a more in-depth comparison between theoretical and experimental band-gap energy difficult. In addition, a band-gap value for Zn_2SiO_4 was calculated in the region between 2.28 and 4.38 eV for the inverse spinel. All functionals underestimate the experimental band-gap energy by 2.51% to 47.66%, except for the B3LYP functional, which overestimates the experimental band-gap energy by 0.54%. Moreover, the band-gap values for Zn_2SnO_4 were calculated to be around 1.04 to 3.60 eV. It was noted that all functionals underestimate the experimental band-gap energy by 10.26% to 68.66%, except for the PBE0 functional, which overestimates the experimental band-gap energy by 8.22%. However, no experimental result has been reported for Zn_2GeO_4, therefore making a more profound analysis between theoretical and experimental band-gap energies impossible.

Figure 3 shows the mean error percentage calculated for the HSE06 hybrid functional successfully predicting the semiconductor behavior for all spinel oxides. This functional has shown better proximity concerning the experimental results, and therefore, it was selected for use in the electronic and vibrational properties.

It is essential to clarify that experimental measurements for band-gap energies of the $ZnIn_2O_4$ and Zn_2GeO_4 materials have not been reported to date. However, the electronic properties in such materials suggest a semiconductor behavior following the electronic results reported for other spinel oxides. In particular, the band-gap energies for such materials are predicted to be around 1.83 to 4.28 eV for $ZnIn_2O_4$ and 1.47 to 4.12 eV for Zn_2GeO_4, respectively.

The electronic structure for ZnX_2O_4 (X = Al, Ga, and In) in the normal spinel structure has been previously reported using DFT/GGA and LDA, where such results showed that $ZnAl_2O_4$ and $ZnIn_2O_4$ have Γ-Γ direct band-gaps of 3.49 and 1.00 eV, respectively,[68] while $ZnGa_2O_4$ has been cited with a K-Γ indirect band-gap of 1.96 eV.[68] Furthermore, a DFT/LDA calculation for the $ZnAl_2O_4$ normal spinel was reported with a Γ-Γ direct band-gap of 4.25 eV. These results underestimate the experimental band-gap energy by 36.03% for $ZnAl_2O_4$ (experimental band-gap 6.05 eV[103]) and 48.26% for $ZnGa_2O_4$ (experimental bang-gap 4.62 eV[5]). However, for the $ZnGa_2O_4$ and $ZnIn_2O_4$ materials simulated by the DFT/LDA approach, the band-gap results were cited as indirect band-gaps at Γ-K direction with 2.82 and 1.71 eV.[17]

Figure 4A-C represents the band structure and the total and projected DOS for ZnX_2O_4 (X = Al, Ga, and In) normal spinel, while Figure 4D-F shows the same results for the ZnM_2O_4 (M = Si, Ge, and Sn) inverse spinel.

The valence band maximum (VBM) and conduction band minimum (CBM) for $ZnAl_2O_4$ are located at the Γ point; therefore, the calculated direct band-gap is 6.19 eV (Figure 4a). This value is only 0.14 eV (2.3%) greater than the experimental value (6.05 eV),[103] whereas $ZnGa_2O_4$ and $ZnIn_2O_4$ have an indirect (L-Γ) band-gap of 4.68 and 3.61 eV, respectively (see Figure 4B,C). The experimental band-gap for $ZnGa_2O_4$ is about 4.62 eV.[5] It is possible to estimate the band-gap energy for Zn_2SiO_4, Zn_2GeO_4, and Zn_2SnO_4 from Figure 4D-F. Such materials have an L-Γ indirect band-gap (see Figure 4D,E), while Zn_2SnO_4 has a Γ-Γ direct band-gap (Figure 4F). Unfortunately, no experimental band-gap energy for the $ZnGe_2O_4$ was found in the literature; therefore, this estimation remains purely theoretical, while the band-gap energies of 4.36 eV[104] and 3.33 eV[105] were experimentally found for Zn_2SiO_4 and Zn_2SnO_4, respectively.

An analysis of the atomic orbital valence has indicated that the upper VBM is predominantly formed from oxygen ($2p_x$, $2p_y$, and $2p_z$) atomic orbitals, and 4s mainly form the bottom of the CBM, 4p (x, y, and z), and 4d (xz, xy, yz, z^2, x^2-y^2) states from the Zn atom. In the case of $ZnAl_2O_4$, 3s and 3p states from Al atoms are hybridized with the O 2p states and Zn 4s, 4p states. In the CBM, the replacement of Al by Ga and In brings contributions from 4s, 4p
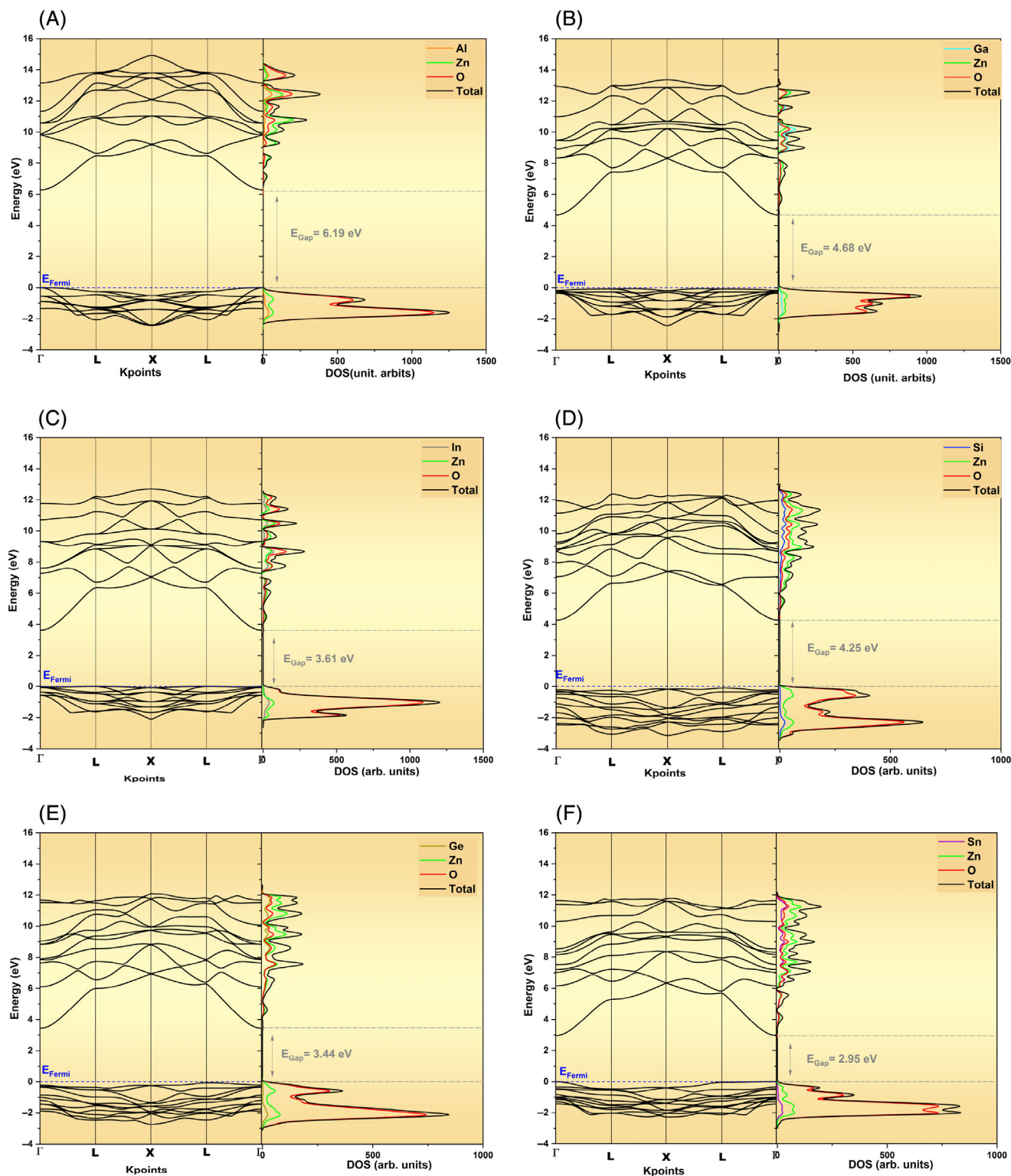
FIGURE 4 Calculated HSE06 band structures and the projected DOS on atoms for (A) $ZnAl_2O_4$, (B) $ZnGa_2O_4$, (C) $ZnIn_2O_4$ normal spinel and (D) Zn_2SiO_4, (E) Zn_2GeO_4, and (F) Zn_2SnO_4 inverse spinel

of Ga atoms and, subsequently, 5s, 5p of In atoms. On the other hand, 3d from Ga and 4d from In atoms contributed to the VBM in $ZnGa_2O_4$ and $ZnIn_2O_4$, respectively. Thus, an inspection of the DOS profiles for ZnX_2O_4 (X = Al, Ga, and In) shows that a new electronic structure between the VBM and CBM originates from 3d Al and 4d In states (Figures 4A-C). The band-gap energy decreases in ZnX_2O_4 when X moves down the group ($ZnAl_2O_4$ > $ZnGa_2O_4$ > $ZnIn_2O_4$), which is associated with the valence atomic states of Ga and In atoms. In addition, Figure 4D-F depicts similar results for Zn_2MO_4 (M = Si, Ge, and Sn) inverse spinels with band-gap energy following the Zn_2SiO_4 > Zn_2GeO_4 > Zn_2SnO_4 sequence.

In terms of optical applications, the band-gaps energy in these structures offers attractive effects. In this context, the spinel-based metal oxide semiconductors are promising candidates for technological applications once the hole or electron carrier is provided to adjust the carrier type and concentration to effectively control the optical, electrical, and magnetic properties of new semiconductor materials. For instance, the band-gap energy range of $ZnGa_2O_4$ (normal) and Zn_2SnO_4 (inverse), examples of metal oxide spinel class, can reduce or improve its efficiency for catalysis, luminescent, and other photo-induced properties to exhibit superior performance on technological devices. Furthermore, the obtained band-gap values (Figure 4) indicate that investigated Zn-based spinel oxides are wide band-gap materials. This class of materials contains widespread candidates for electronic applications, mainly associated with the high-voltage, high-temperature, and high-frequency electronic devices.[106-108] Furthermore, wide band-gap materials can be applied as UV optoelectronics and UV-transparent devices, emerging as a potential candidate for applications in different fields.[109,110]

3.3 | Vibrational properties

According to group theory, cubic spinels with space group O_h^7, *Fd-3m* (227), have the following phonon modes at the Γ point (Raman + infrared):

$$\Gamma = A_{1g}(R) + E_g(R) + F_{1g} + 3F_{2g}(R) + 2A_{2u} + 2E_u + 5F_{1u}(IR) + 2F_{2u}$$

with A_{1g}, E_g, and F_{2g} being the Raman-active modes, whereas F_{1u} are the active vibrational modes in the infrared spectra. The $E_{(g, u)}$ and $F_{(1g, 2g, 1u, 2u)}$ modes are doubly and triply degenerated, respectively, and one triply degenerated F_{1u} corresponds to acoustic modes. The three Raman-actives F_{2g} modes are labeled F_{2g} (1), F_{2g} (2), and F_{2g} (3), where F_{2g} (1) is associated with the lowest Raman shift, and F_{2g} (3) indicates the Raman mode with the highest wavenumber.[111] Because the spinel structure has an inversion symmetry element, the active modes are mutually exclusive. Thus, the vibrational modes are either infrared (IR) or Raman active but not both.

Furthermore, the irreducible representations to describe the normal modes of the vibrational modes associated with each atomic species in their Wyckoff positions are:

$$8a\,[T] : F_{2g}(R) + F_{1u}(IR)$$

$$16d\,[M] : A_{2u} + E_u + 2F_{1u}(IR) + F_{2u}$$

$$32e\,[X] : A_{1g}(R) + E_g(R) + F_{1g} + 2F_{2g}(R) + A_{2u} + E_u + 2F_{1u}(IR) + F_{2u},$$

where R and IR correspond to Raman- and infrared-active modes, respectively.

Table 2 summarizes the calculated and experimental Raman modes. Hence, only five modes $A_{1g} + E_g + 3F_{2g}$ should be observed in the Raman spectra of normal spinels. In addition, good agreement was found between calculated and experimentally measured Raman mode frequencies. The data generally and favorably compare (within 2-4) with the values from our calculations. The most significant difference, which occurred in the Eg mode, is about 2.7% for $ZnAl_2O_4$, and $ZnGa_2O_4$ showed a discrepancy of about 0.5% to 3.2% in error mode frequencies compared to the experimental results.

Analyzing the obtained Raman wavenumbers in the normal spinel oxides, it was possible to examine the role of X cations on vibrational properties. For $ZnAl_2O_4$, the low-frequency motions (197 cm^{-1}) are connected to Zn and Al ions, while the phonon modes with higher frequencies (above 700 cm^{-1}) are attributed to the stretching vibrations on the oxygen tetrahedral. On the other hand, the frequencies observed at ~518 cm^{-1} are characteristic of the stretching vibrations of the oxygen atom in the octahedral environment.[114]

In the case of $ZnGa_2O_4$, frequencies below 393 cm^{-1} are dominated by the motion of Zn and Ga atoms, while the motion of O ions dominates higher frequencies, as in $ZnAl_2O_4$. The main difference between the two compounds is because Ga atoms are heavier than Al atoms. Thus, we have found good agreement between the calculated phonon spectrum and experimental frequencies for all materials.

Experimental frequencies for $ZnIn_2O_4$ materials have not been reported yet. However, according to the group theory calculations and symmetry for Zn and In crystals with a spinel-type cubic structure, we can identify five (176, 386, 436, 579, and 645 cm^{-1}) theoretical Raman-active vibrational modes for $ZnIn_2O_4$. Aiming to predict the Raman spectrum for $ZnIn_2O_4$ material, Figure 5 illustrates the theoretical Raman spectrum obtained with CRYSTAL17,[76] where two high-intensity bands centered at 386 and 645 cm^{-1} are present in theoretical Raman spectrum, which correspond to intense peaks in the Raman E_g and A_{1g} modes, respectively.

Table 3 summarizes the experimental and theoretical results for the Raman modes of Zn_2SnO_4. Experimentally, two and three of the expected five Raman-active modes were also found. Other modes were also found at 107 and 148 cm^{-1}. The inverse spinel structure of Zn_2SnO_4 following the total number of active and inactive infrared reflection and Raman modes are:

TABLE 2 Calculated Raman frequencies from the HSE06 functional and experimental Raman active modes (cm^{-1}) for normal spinel oxides

| Spinel compounds | Modes | | | | | Reference |
	F_{2g}	E_g	F_{2g}	F_{2g}	A_{1g}	
$ZnAl_2O_4$	201	430	518	669	789	This work
Others works	196	417	509	658	758	[111]
	197	442	520	665	785	[112]
	—	411	510	661	—	[113,114]
	—	420	509	659	—	[115]
$ZnGa_2O_4$	192	393	483	627	729	This work
Others works	—	—	462	606	706	[89]
	186	395	488	618	717	[116]
	—	638	467	611	714	[116]

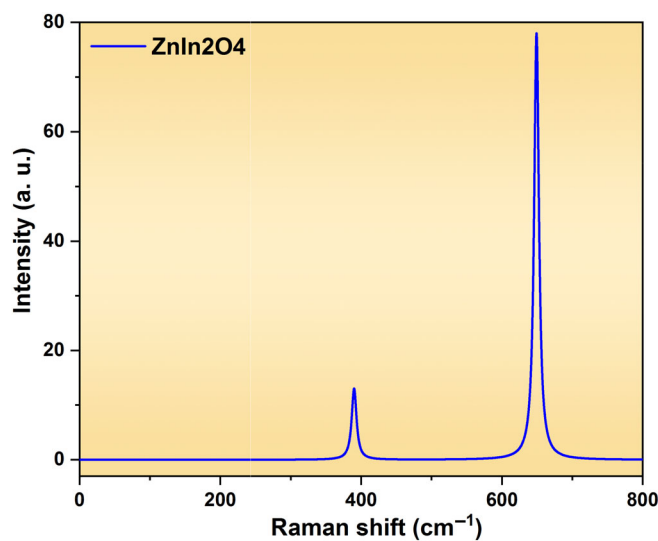**FIGURE 5** Theoretical Raman spectra predicted for $ZnIn_2O_4$ material

TABLE 3 Calculated Raman frequencies from the HSE06 functional and experimental Raman-active modes (cm^{-1}) for inverse spinel oxides

| Spinel compounds | Modes | | | | | | | | | | | | | | | References |
	A_g	B_{2g}	B_{3g}	B_{1g}	B_{3g}	A_g	B_{2g}	B_{1g}	B_{3g}	B_{2g}	A_g	B_{3g}	A_g	B_{2g}	A_g	
Zn_2SnO_4	169	169.8	175	276	289	328	374	424	453	462	499	521	557	625	665	This work
Other works			F_{2g}		E_g		F_{2g}		F_{2g}		A_{1g}					
			—		—		—		541		673					[121]
			—		—		—		528		668					[118,120]
			—		—		437		526		667					[122]
			381		467		527		556		667					[123]
	148		226		375		435		526		667					[124]
	107		224		—		—		528		668					[124]

$$\Gamma = 1A_{1g} + 1E_g + 3F_{2g} + 7F_{1u},$$

where $1A_{1g}$, $1E_g$, and $3F_{2g}$ represent the five first-order active Raman modes, while $7F_{1u}$ represents the infrared modes. As one IR mode is inactive, there are six IR active infrared modes (F_{1u}) for zinc stannate with a cubic inverse nondefective Zn_2SnO_4 spinel structure. The phonon mode located at 526 to 582 cm^{-1} corresponds to the F_{2g} symmetric bending of oxygen atoms in the M − O bonds of the [MO$_6$] octahedra (M = Zn or Sn). In addition, the intense Raman band at about 667 cm^{-1} is assigned to the A_{1g} symmetric stretching vibration of the Zn − O bonds in the [ZnO$_4$] tetrahedra of inverse Zn_2SnO_4 spinel. The data are in accordance with the values reported in the literature.[117–120]

Nevertheless, five Raman modes (F_{2g} (1), E_g, F_{2g} (2), F_{2g} (3), and A_{1g}) for the Zn_2SnO_4 inverse spinel structure present changes because of the inversion degree; therefore, the symmetry and the normal mode number are increased. This evidence supports a breaking in the degeneracy by the transformation of the F_{2g} mode into (B_{2g} + E_g) and E_g into (A_{1g} + B_{1g}) modes. Therefore, we consider that the E_g and A_{1g} modes are transformed into A_g mode, whereas the F_{2g} (1), F_{2g} (2), and F_{2g} (3) modes become B_{1g}, B_{2g}, B_{3g} modes, respectively, as reported in references.[63,125] Besides, P. R. Graves et al and C. Haas[126,127] have stated that many subgroups originated from a reduction in the O_h higher symmetry. Such a loss of symmetry can be associated with the lattice defects or ordering of the metallic ions on their sites.

The experimental Raman spectrum for cubic Zn_2SiO_4 and Zn_2GeO_4 structures have not been reported so far. In this context, the theoretical Raman spectrum for both Zn_2SiO_4 and Zn_2GeO_4 structures were calculated, as reported in Figure 6. The corresponding representation for the inverse cubic symmetry is composed of 15 (169, 195, 202, 328, 345, 373, 390, 409, 422, 519, 556, 624, 672, 706, 767 cm^{-1} for Zn_2SiO_4 and 172, 188, 189, 315, 332, 370, 377, 386, 432, 491, 524, 575, 620, 666, and 721 cm^{-1} for Zn_2GeO_4) theoretical Raman-active modes predicted by group theory. However, the obtained theoretical Raman spectrum indicates the presence of four and five more intense bands for Zn_2GeO_4 and Zn_2SiO_4, respectively, which can be associated with the accommodation of Ge and Si atoms along with octahedral sites of inverse spinel structure.

3.4 | Cohesive Energy

The computer-aided materials design is strictly associated with the analysis of structural, electronic, vibrational, and energetics properties of investigated candidates.[128–130] Here, in order to investigate the thermodynamic stability of investigated Zn-based spinels, the cohesive energy (E_{coh}) was calculated as:

$$E_{coh} = E_{bulk}(Zn_xM_yO_4) - \sum_a^N E_i,$$

where E_{bulk} is the total energy for $Zn_xM_yO_4$ oxide, E_i is the total energy for each atom (i) belonging to the crystal unit cell, and N is the number of atoms in the unit cell.

For the normal spinel structure, the calculated values at the HSE06 level of theory follow the order -1.29 eV atom^{-1} ($ZnAl_2O_4$) < -2.15 eV atom^{-1} ($ZnGa_2O_4$) < -2.67 eV atom^{-1} ($ZnIn_2O_4$). On the other hand, for the inverse Zn-based spinels, the E_{coh} order was calculated as -1.17 eV atom^{-1} (Zn_2GeO_4) < -1.20 eV atom^{-1} (Zn_2SnO_4) < -1.43 eV atom^{-1} (Zn_2SiO_4). At first glance, it was observed that all investigated Zn-based spinel oxides exhibit negative E_{coh} values, indicating a thermodynamic stability with regard to their containing atoms. In addition, the obtained results indicate larger E_{coh} values for normal spinels, indicating that the inversion of Zn cations induces a structural disorder for inverse spinels addressed to the cation accommodation in both tetrahedral and octahedral sites of the spinel structure.

Furthermore, it was noted that, when moving from Al to In, the E_{coh} increases for normal spinels, indicating an increased stability associated with the accommodation of Al, Ga, and In cations along the octahedral sites. On the other hand, moving from Si to Ge, the E_{coh} reduces for the inverse spinel, confirming the role of Zn cation distribution in the structural stability. In this case, the bigger the B-site cation (Sn > Ge > Si), the smaller the E_{coh} becomes, indicating a structural competition for octahedral sites.
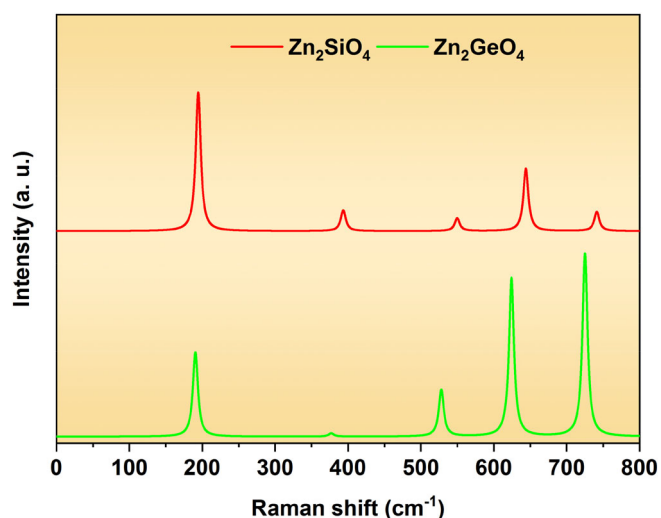

FIGURE 6 Theoretical Raman spectra predicted for Zn_2SiO_4 and Zn_2SiO_4 materials

Therefore, the combination of stability, structural, electronic, and vibrational properties of Zn-based spinel oxides can be addressed to the physical and chemical features of M cations (M = Al, Ga, In, Si, Ge, Sn) as ionic radii, site accommodation, and valence orbitals.

4 | CONCLUSION

In summary, we have performed first-principles calculations to study structural, electronic, and vibrational properties for the normal ZnX_2O_4 (X = Al, Ga, and In) and inverse Zn_2MO_4 (M = Si, Ge, and Sn) cubic spinel materials. Furthermore, the role of exchange-correlation treatment for the prediction of spinel properties was investigated comparing HSE06, PBE0, B3LYP, and PBESol functionals. Indeed, hybrid DFT/HF functionals are better for all investigated properties of the investigated spinel oxides, with HSE06 being the formalism with the best performance, overcoming previous theoretical studies. Moreover, the systematic exchange-correlation functional investigation validates the mightiness of hybrid DFT/HF treatment to successfully predict the spinel properties. In this context, the role of cation replacement on the main properties of spinel oxides was discussed through site accommodation, ionic radii, and structural disorders that govern the electronic structure and vibrational features of normal and inverse spinel structures. We hope that this work can stimulate future developments in the line of the spinel materials with unique properties.

AUTHOR CONTRIBUTIONS

Marisa Oliveira: Conceptualization; formal analysis; investigation; writing-original draft; writing-review and editing. **Renan Ribeiro:** Conceptualization; formal analysis; investigation; writing-original draft; writing-review and editing. **Mauricio Bomio:** Investigation; supervision; writing-original draft; writing-review and editing. **Elson Longo:** Investigation; supervision; writing-original draft; writing-review and editing. **Sergio de Lazaro:** Conceptualization; formal analysis; investigation; resources; supervision; writing-original draft; writing-review and editing.

CONFLICT OF INTEREST

The authors declare that there is no conflict of interest regarding the publication of this article.

ORCID

Marisa C. Oliveira https://orcid.org/0000-0003-3392-7489

Renan A. P. Ribeiro https://orcid.org/0000-0002-4128-8296

REFERENCES

[1] K. E. Sickafus, J. M. Wills, N. W. Grimes, *J. Am. Ceram. Soc.* **1999**, *82*, 3279.
[2] N. W. Grimes, *Phys. Technol.* **1975**, *6*, 22.
[3] M. A. Lahmer, *Comput. Condens. Matter.* **2019**, *20*, e00387.
[4] S. Sommer, E. D. Bøjesen, H. Reardon, B. B. Iversen, *Cryst. Growth Des.* **2020**, *20*, 1789.
[5] T. A. Safeera, R. Khanal, J. E. Medvedeva, A. I. Martinez, G. Vinitha, E. I. Anila, *J. Alloy Compd.* **2018**, *740*, 567.
[6] P. Loiko, A. Belyaev, O. Dymshits, I. Evdokimov, V. Vitkin, K. Volkova, M. Tsenter, A. Volokitina, M. Baranov, E. Vilejshikova, A. Baranov, A. Zhilin, *J. Alloy Compd.* **2017**, *725*, 998.
[7] L. A. Diaz-Torres, A. I. Mtz-Enriquez, C. R. Garcia, E. Coutino-Gonzalez, A. I. Oliva, M. A. Vallejo, T. Cordova, C. Gomez-Solis, J. Oliva, *Renew. Energy* **2020**, *152*, 634.
[8] Y. Zhang, Z. Wu, D. Geng, X. Kang, M. Shang, X. Li, H. Lian, Z. Cheng, J. Lin, *Adv. Func. Mater.* **2014**, *24*, 6581.
[9] J. Liang, Y. Chai, L. Li, D. Li, J. Shen, Y. Zhang, X. Wang, *Appl. Catal. B-Environ.* **2020**, *265*, 118551.
[10] Q. Li, L. Zhang, C. Tang, P. Zhao, C. Yin, J. Yin, *Int. J. Hydrogen Energy* **2020**, *45*, 6621.
[11] S. S. Nalimova, A. I. Maksimov, L. B. Matyushkin, V. A. Moshnikov, *Glass Phys. Chem.* **2019**, *45*, 251.
[12] S.-W. Yang, F. Peng, W.-T. Li, Q.-W. Hu, X.-Z. Yan, L. Lei, X.-D. Li, D.-W. He, *Chin. Phys. B* **2016**, *25*, 076101.
[13] M. Masjedi-Arani, M. Salavati-Niasari, *Int. J. Hydrogen Energy* **2017**, *42*, 858.
[14] P. P. Das, A. Roy, S. Agarkar, P. S. Devi, *Dyes Pigments* **2018**, *154*, 303.
[15] A. K. Kushwaha, *Comp. Mater. Sci.* **2014**, *85*, 259.
[16] L. Pisani, T. Maitra, R. Valentí, *Phys. Rev. B* **2006**, *73*, 205204.
[17] H. Dixit, N. Tandon, S. Cottenier, R. Saniz, D. Lamoen, B. Partoens, V. Van Speybroeck, M. Waroquier, *New J. Phys.* **2011**, *13*, 063002.

[18] W. Mekprasart, K. Boonyarattanakalin, W. Pecharapa, K. N. Ishihara, *Mater. Today: Proc.* **2018**, *5*, 14126.

[19] F. Z. Akika, M. Benamira, H. Lahmar, M. Trari, I. Avramova, Ş. Suzer, *Surf. Interfaces* **2020**, *18*, 100406.

[20] M. M. Golsheikh, A. M. Arabi, M. S. Afarani, *Mater. Res. Express* **2019**, *6*, 125052.

[21] K. Buvaneswari, G. Vetha, V. Andal, *Int. J. Chem. Tech. Res.* **2015**, *8*, 06.

[22] S. V. Motloung, K. G. Tshabalala, R. E. Kroon, T. T. Hlatshwayo, M. Mlambo, S. Mpelane, *J. Mol. Struct.* **2019**, *1175*, 241.

[23] T. Ishinaga, T. Iguchi, H. Kominami, K. Hara, M. Kitaura, A. Ohnishi, *Phys. Status Solidi C* **2015**, *12*, 797.

[24] M. K. Hussen, F. B. Dejene, G. G. Gonfa, *Appl. Phys. A* **2018**, *124*, 390.

[25] X. Duan, J. Liu, Y. Wu, F. Yu, X. Wang, *J. Lumin.* **2014**, *153*, 361.

[26] T. Zhang, A. Du, C. Chen, X. Ji, B. Zhou, J. Shen, Z. Zhang, *RSC Adv.* **2019**, *9*, 33883.

[27] A. Fernández-Osorio, M. Tapia, A. R. Vázquez-Olmos, J. Chávez, *J. Solid State Chem.* **2019**, *269*, 328.

[28] X. Lu, Z. Du, B. Quan, W. Bian, H. Zhu, Q. Zhang, *J. Mater. Chem. C* **2019**, *7*, 8261.

[29] X. Li, X. Zhang, X. Zheng, Y. Shao, M. He, P. Wang, X. Fu, D. Li, *J. Mater. Chem. A* **2014**, *2*, 15796.

[30] M. Zhong, Y. Ma, P. Oleynikov, K. Domen, J.-J. Delaunay, *Energy Environ. Sci.* **2014**, *7*, 1693.

[31] B. C. Babu, S. Buddhudu, *Indian J. Phys.* **2014**, *88*, 631.

[32] R. B. Basavaraj, J. Malleshappa, G. P. Darshan, B. D. Prasad, H. Nagabhushana, *AIP Conf. Proc.* **2018**, *1942*, 050090.

[33] R. B. Basavaraj, H. Nagabhushana, B. Daruka Prasad, S. C. Sharma, S. C. Prashantha, B. M. Nagabhushana, *Optik* **2015**, *126*, 1745.

[34] B. C. Babu, G.-G. Wang, B. Yan, Q. Yang, A. P. Baker, *Ceram. Int.* **2018**, *44*, 938.

[35] S. Lee, B. Jeon, T. Kang, W. Lee, A. M. Malik, S. Park, J. Lim, B. Park, Y. Jeong, J. Kim, *J. Lumin.* **2018**, *196*, 290.

[36] Y. Mei, H.-B. Jiang, D.-F. Chen, W.-C. Zheng, *J Lumin* **2019**, *212*, 180.

[37] X.-Y. Sun, Z. He, X. Gu, *J. Mater. Sci. Mater. Electron.* **2018**, *29*, 17217.

[38] F. Chi, X. Wei, B. Jiang, Y. Chen, C. Duan, M. Yin, *Dalton Trans.* **2018**, *47*, 1303.

[39] Y. Qi, L. Zhao, W. Bian, X. Yu, X. Xu, J. Qiu, *Chin. Opt. Lett.* **2017**, *15*, 081601.

[40] Y. Li, A. Zhao, C. Chen, C. Zhang, J. Zhang, G. Jia, *Dyes Pigments* **2018**, *150*, 267.

[41] W. Fang, K. Cheng, H. Xiang, Y. Tang, Y. Zhai, C. Su, L. Fang, *J. Alloy Compd.* **2019**, *799*, 495.

[42] X. Gao, C. Li, S. Li, H. Zhang, Z. Li, Y. Hong, J. Sun, *J. Lumin.* **2017**, *190*, 457.

[43] D. Bauer, T. E. Ashton, A. R. Groves, A. Dey, S. Krishnamurthy, N. Matsumi, J. A. Darr, *Energy Technol.* **2020**, *8*, 1900692.

[44] Z. Wang, Z. Tang, X. Peng, C. Xia, F. Wang, *Int. J. Mod. Phys. B* **2019**, *33*, 1950389.

[45] N. M. Cao Hoang Phuong Lan, C. X. Thang, V.-H. Pham, P. The Kien, V. T. Ngoc Minh, T. T. Hao Tam, *Optik* **2019**, *199*, 163310.

[46] H. He, Y. Zhang, Q. Pan, G. Wu, G. Dong, J. Qiu, *J. Mater. Chem. C* **2015**, *3*, 5419.

[47] F. Chi, B. Jiang, Z. Zhao, Y. Chen, X. Wei, C. Duan, M. Yin, W. Xu, *Sens. Actuators, B: Chem.* **2019**, *296*, 126640.

[48] L. Jiang, *J Photoch Photobio A-Chem* **2019**, *377*, 282.

[49] H. Yao, Y. Zhang, Y. Xu, *J Alloy Compd* **2019**, *770*, 149.

[50] M. Li, Z. Zhang, X. Ge, Z. Wei, Y. Yao, H. Chen, C. Wang, F. Du, G. Chen, *Chem Eng J* **2018**, *331*, 203.

[51] V. Y. Suzuki, L. H. C. Amorin, N. M. Lima, E. G. Machado, P. E. Carvalho, S. B. R. Castro, C. C. S. Alves, A. P. Carli, M. S. Li, E. Longo, F. A. La Porta, *J Mater Chem C* **2019**, *7*, 8216.

[52] M. Mary Jaculine, C. Justin Raj, S. Jerome Das, *J Alloy Compd* **2013**, *577*, 131.

[53] M. Zhang, X. Cui, Y. Wang, B. Wang, M. Ye, W. Wang, C. Ma, Z. Lin, *Nano Energy* **2020**, *71*, 104620.

[54] S. S. Shin, W. S. Yang, J. H. Noh, J. H. Suk, N. J. Jeon, J. H. Park, J. S. Kim, W. M. Seong, S. I. Seok, *Nat Commun* **2015**, *6*, 7410.

[55] Z. Wang, A. Sackmann, S. Gao, U. Weimar, G. Lu, S. Liu, T. Zhang, N. Barsan, *Sens. Actuators, B: Chem.* **2019**, *285*, 590.

[56] K. Kim, A. Annamalai, S. H. Park, T. H. Kwon, M. W. Pyeon, M.-J. Lee, *Electrochim. Acta* **2012**, *76*, 192.

[57] K. Al-Attafi, F. H. Jawdat, H. Qutaish, P. Hayes, A. Al-Keisy, K. Shim, Y. Yamauchi, S. X. Dou, A. Nattestad, J. H. Kim, *Nano Energy* **2019**, *57*, 202.

[58] M. Shojaeifar, M. Asemi, E. Mohajerani, M. Ghanaatshoar, *Curr. Appl. Phys.* **2020**, *20*, 358.

[59] S. Silvestri, J. F. de Oliveira, E. L. Foletto, *Mater. Res. Bull.* **2019**, *117*, 56.

[60] S. Silvestri, R. dos Santos Trentin, J. da Silveira Salla, E. L. Foletto, *Water Air Soil Pollut.* **2019**, *230*, 186.

[61] M. Fakhrzad, A. H. Navidpour, M. Tahari, S. Abbasi, *Mater. Res. Express* **2019**, *6*, 095037.

[62] S. Silvestri, N. Stefanello, J. da Silveira Salla, E. L. Foletto, *Res. Chem. Intermed.* **2019**, *45*, 4299.

[63] P. P. Das, P. S. Devi, D. A. Blom, T. Vogt, Y. Lee, *ACS Omega* **2019**, *4*, 10539.

[64] M. A. Lahmer, *Surf. Sci.* **2018**, *669*, 189.

[65] M. E. Striefler, G. R. Barsch, *J. Phys. Chem. Solids* **1972**, *33*, 2229.

[66] M. Marinelli, S. Baroni, F. Meloni, *Phys. Rev. B* **1988**, *38*, 8258.

[67] H. D. Lutz, J. Himmrich, H. Haeuseler, *Z. Naturforsch.* **1990**, *45a*, 893.

[68] F. Zerarga, A. Bouhemadou, R. Khenata, S. Bin-Omran, *Solid State Sci.* **2011**, *13*, 1638.

[69] L. Zhang, G.-F. Ji, F. Zhao, Z.-Z. Gong, *Chin. Phys. B* **2011**, *20*, 047102.

[70] A. D. Becke, *J. Chem. Phys.* **1993**, *98*, 5648.

[71] C. Lee, W. Yang, R. G. Parr, *Phys. Rev. B* **1988**, *37*, 785.

[72] A. V. Krukau, O. A. Vydrov, A. F. Izmaylov, G. E. Scuseria, *J. Chem. Phys.* **2006**, *125*, 224106.

[73] C. Adamo, V. Barone, *J. Chem. Phys.* **1999**, *110*, 6158.

[74] J. P. Perdew, A. Ruzsinszky, G. I. Csonka, O. A. Vydrov, G. E. Scuseria, L. A. Constantin, X. Zhou, K. Burke, *Phys. Rev. Lett.* **2008**, *100*, 136406.

[75] J. P. Perdew, A. Ruzsinszky, G. I. Csonka, O. A. Vydrov, G. E. Scuseria, L. A. Constantin, X. Zhou, K. Burke, *Phys. Rev. Lett.* **2009**, *102*, 039902.

[76] R. Dovesi, A. Erba, R. Orlando, C. M. Zicovich-Wilson, B. Civalleri, L. Maschio, M. Rérat, S. Casassa, J. Baima, S. Salustro, B. Kirtman, *Wiley Inter. Rev.: Comp. Mol. Sci.* **2018**, *8*, e1360.

[77] H. J. Monkhorst, J. D. Pack, *Phys. Rev. B* **1976**, *13*, 5188.

[78] T. Homann, U. Hotje, M. Binnewies, A. Börger, K.-D. Becker, T. Bredow, *Solid State Sci.* **2006**, *8*, 44.

[79] M. Catti, G. Valerio, R. Dovesi, M. Causà, *Phys. Rev. B* **1994**, *49*, 14179.

[80] R. Pandey, M. Causa, N. M. Harrison, M. Seel, *J. Phys.: Condens. Matter.* **1996**, *8*, 3993.

[81] R. Nada, C. R. A. Catlow, R. Dovesi, C. Pisani, *Phys. Chem. Miner.* **1990**, *17*, 353.

[82] G. Sophia, P. Baranek, C. Sarrazin, M. Rerat, R. Dovesi. Systematic influence of atomic substitution on the phase diagram of ABO3 ferroelectric perovskites, **2014**. https://www.crystal.unito.it/Basis_Sets/germanium.html.

[83] M. F. Peintinger, D. V. Oliveira, T. Bredow, *J. Comput. Chem.* **2013**, *34*, 451.

[84] P. Pernot, B. Civalleri, D. Presti, A. Savin, *J. Phys. Chem. A* **2015**, *119*, 5288.

[85] G. Sophia, P. Baranek, C. Sarrazin, M. Rerat, R. Dovesi. Systematic influence of atomic substitution on the phase diagram of ABO3 ferroelectric perovskites, **2014**. https://www.crystal.unito.it/Basis_Sets/tin.html.

[86] H. S. C. O'Neill, W. A. Dollase, *Phys. Chem. Miner.* **1994**, *20*, 541.

[87] R. J. Hill, J. R. Craig, G. V. Gibbs, *Phys. Chem. Miner.* **1979**, *4*, 317.

[88] D. Levy, A. Pavese, A. Sani, V. Pischedda, *Phys. Chem. Miner.* **2001**, *28*, 612.

[89] S. López, A. H. Romero, P. Rodríguez-Hernández, A. Muñoz, *Phys. Rev. B* **2009**, *79*, 214103.

[90] R. Ianoş, S. Borcănescu, R. Lazău, *Chem. Eng. J.* **2014**, *240*, 260.

[91] S. López-Moreno, A. H. Romero, P. Rodríguez-Hernández, A. Muñoz, *High Press Res.* **2009**, *29*, 573.

[92] S.-H. Wei, S. B. Zhang, *Phys. Rev. B* **2001**, *63*, 045112.

[93] F. Zerarga, A. Bouhemadou, R. Khenata, S. Binomran, *Comput. Mater. Sci.* **2011**, *50*, 2651.

[94] A. Bouhemadou, R. Khenata, *Phys. Lett. A* **2006**, *360*, 339.

[95] S. Z. Karazhanov, P. Ravindran, P. Vajeeston, A. G. Ulyashin, H. Fjellvag, B. G. Svensson, *J. Phys.: Condens. Matter.* **2009**, *21*, 485801.

[96] M. Kanzaki, *J. Miner. Petrol. Sci.* **2018**, *113*, 41.

[97] Y. Syono, S.-I. Akimoto, Y. Matsui, *J. Solid State Chem.* **1971**, *3*, 369.

[98] L. Bao, J. Zang, G. Wang, X. Li, *Nano Lett.* **2014**, *14*, 6505.

[99] I. Saafi, T. Larbi, A. Amlouk, M. Amlouk, *Optik* **2019**, *187*, 49.

[100] Y.-Q. Jiang, X.-X. Chen, R. Sun, Z. Xiong, L.-S. Zheng, *Mater. Chem. Phys.* **2011**, *129*, 53.

[101] X. Ji, X. Huang, J. Liu, J. Jiang, X. Li, R. Ding, Y. Hu, F. Wu, Q. Li, *J. Alloy Compd.* **2010**, *503*, L21.

[102] J. Lee, S.-C. Lee, C. S. Hwang, J.-H. Choi, *J. Mater. Chem. C* **2013**, *1*, 6364.

[103] A. V. Belyaev, I. I. Evdokimov, V. V. Drobotenko, A. A. Sorokin, *J. Eur. Ceram. Soc.* **2017**, *37*, 2747.

[104] S. Z. Karazhanov, P. Ravindran, H. Fjellvåg, B. G. Svensson, *J. Appl. Phys.* **2009**, *106*, 123701.

[105] X. Xin, J. Zhang, C. Chen, G. Li, J. Qin, Z. Yang, H. Lu, J. Gao, C. Wang, Z. He, *J. Alloy Compd.* **2019**, *780*, 228.

[106] P. G. Neudeck, R. S. Okojie, C. Liang-Yu, *Proc. IEEE* **2002**, *90*, 1065.

[107] J. Millán, P. Godignon, X. Perpiñà, A. Pérez-Tomás, J. Rebollo, *IEEE Trans. Power Electron.* **2014**, *29*, 2155.

[108] T. P. Chow, R. Tyagi, *IEEE Trans. Electron. Devices* **1994**, *41*, 1481.

[109] E. Chikoidze, C. Sartel, I. Madaci, H. Mohamed, C. Vilar, B. Ballesteros, F. Belarre, E. del Corro, P. Vales-Castro, G. Sauthier, L. Li, M. Jennings, V. Sallet, Y. Dumont, A. Pérez-Tomás, *Cryst. Growth Des.* **2020**, *20*, 2535.

[110] Y. Jang, S. Hong, J. Seo, H. Cho, K. Char, Z. Galazka, *Appl. Phys. Lett.* **2020**, *116*, 202104.

[111] A. Chopelas, A. M. Hofmeister, *Phys. Chem. Miner.* **1991**, *18*, 279.

[112] C. M. Fang, C. K. Loong, G. A. de Wijs, G. de With, *Phys. Rev. B* **2002**, *66*, 144301.

[113] V. D'Ippolito, G. B. Andreozzi, F. Bosi, U. Hålenius, L. Mantovani, D. Bersani, R. A. Fregola, *Mineral. Mag.* **2013**, *77*, 2941.

[114] V. D'Ippolito, G. B. Andreozzi, D. Bersani, P. P. Lottici, *J. Raman Spectrosc.* **2015**, *46*, 1255.

[115] V. Mohaček-Grošev, M. Vranić, A. Maksimović, V. Mandić, *J. Alloys Compd.* **2017**, *697*, 90.

[116] G. G. P. Van Gorkom, J. H. Haanstra, H. Boom, *J. Raman Spectrosc.* **1973**, *1*, 513.

[117] X. Shen, J. Shen, S. J. You, L. X. Yang, L. Y. Tang, Y. C. Li, J. Liu, H. Yang, K. Zhu, Y. L. Liu, W. Y. Zhou, C. Q. Jin, R. C. Yu, S. S. Xie, *J. Appl. Phys.* **2009**, *106*, 113523.

[118] L. Wang, X. Zhang, X. Liao, W. Yang, *Nanotechnology* **2005**, *16*, 2928.

[119] Z. Chen, M. Cao, C. Hu, *J. Phys. Chem. C* **2011**, *115*, 5522.

[120] M. Ben Ali, F. Barka-Bouaifel, B. Sieber, A. Addad, L. Boussekey, M. Férid, R. Boukherroub, *J Colloid Interface Sci.* **2015**, *457*, 360.

[121] A. Singhal, B. Vishwanadh, *ChemistrySelect* **2018**, *3*, 13432.

[122] S. Yang, J. Zhang, *Chem. Phys. Lett.* **2018**, *712*, 40.

[123] V. Šepelák, S. M. Becker, I. Bergmann, S. Indris, M. Scheuermann, A. Feldhoff, C. Kübel, M. Bruns, N. Stürzl, A. S. Ulrich, M. Ghafari, H. Hahn, C. P. Grey, K. D. Becker, P. Heitjans, *J. Mater. Chem. C* **2012**, *22*, 3117.

[124] M. V. Nikolić, T. Ivetić, D. L. Young, K. M. Paraskevopoulos, T. T. Zorba, V. Blagojević, P. M. Nikolić, D. Vasiljević-Radović, M. M. Ristić, *Mater. Sci. Eng. B* **2007**, *138*, 7.

[125] Z. Wang, D. Schiferl, Y. Zhao, H. S. C. O'Neill, *J. Phys. Chem. Solids* **2003**, *64*, 2517.

[126] P. R. Graves, C. Johnston, J. J. Campaniello, *Mater. Res. Bull.* **1988**, *23*, 1651.

[127] C. Haas, *J. Phys. Chem. Solids* **1965**, *26*, 1225.

[128] J. A. Santana, J. T. Krogel, P. R. C. Kent, F. A. Reboredo, *J. Chem. Phys.* **2016**, *144*, 174707.

[129] K. Tan, M. Dixit, J. Dean, G. Mpourmpakis, *Ind. Eng. Chem. Res.* **2019**, *58*, 20236.

[130] R. Pandey, J. D. Gale, S. K. Sampath, J. M. Recio, *J. Am. Ceram. Soc.* **1999**, *82*, 3337.